

SUPPLEMENTARY INFORMATION

**First steps towards a stable neon compound: Observation
and bonding analysis of $[B_{12}(CN)_{11}Ne]^-$**

Martin Mayer, Markus Rohdenburg, Valentin van Lessen, Marc C. Nierstenhöfer, Edoardo Aprà, Simon Grabowsky, Knut R. Asmis, Carsten Jenne,* Jonas Warneke*

Table of contents

S 1 Synthesis and characterization of $[PPh_4]_2[B_{12}(CN)_{12}]$ (p. S2)

S 1.1 Experimental section (p. S2)

S 1.2 Synthesis of $[PPh_4]_2[B_{12}(CN)_{12}]$ (p. S5)

S 1.3 NMR spectroscopy (p. S6)

S 1.4 Vibrational spectroscopy (p. S9)

S 1.5 Mass spectrometry (p. S12)

S 1.6 Crystal structure of $[PPh_4]_2[B_{12}(CN)_{11.5}I_{0.5}]$ (p. S13)

S 2 Details theoretical determination of Ne and He attachment enthalpies to $[B_{12}(CN)_{11}]^-$ (p. 15)

S 3 Ion molecule reactions of $[B_{12}(CN)_{11}]^-$ with He and Ne (p. S18)

S 3.1 Experimental details (p. S18)

S 3.2 TOF mass spectra $[B_{12}(CN)_{11}Ne]^-$ (p. S18)

S 4 Energy decomposition analysis (p. S19)

S 4.1 Method details (p. S19)

S 4.2 Bond parameters of the B-Ne bond in $Na[B_{12}(CN)_{11}Ne]$ (p. S20)

S 5 Cartesian coordinates of all optimized geometries (p. S22)

S 6 Supplementary references (p. S25)

S 1 Synthesis and characterization of $[\text{PPh}_4]_2[\text{B}_{12}(\text{CN})_{12}]$

S 1.1 Experimental section

General remarks: The solvents acetonitrile (AWD Scientific), dimethyl sulfoxide (Roth) and CD_3CN (Fisher Scientific) are commercially available and were used without further purification. KCN (VWR Chemicals, 98 %) is a commercial product and was used without further purification. The weakly coordinating anion $[\text{B}_{12}\text{I}_{12}]^{2-}$ was synthesized from the *closo*-dodecaborate¹ $[\text{B}_{12}\text{H}_{12}]^{2-}$ with iodine and iodine monochloride by a published procedure.²

IR spectroscopy: IR spectra were recorded on a Bruker VERTEX 70 spectrometer equipped with a diamond ATR attachment in the range of 400–4000 cm^{-1} .

Raman spectroscopy: Raman spectra were recorded in flame sealed capillaries on a Bruker MultiRam spectrometer in the range of 100–3600 cm^{-1} .

NMR spectroscopy: ^1H , ^{11}B and ^{31}P NMR spectra were measured on a Bruker Avance 400 MHz NMR spectrometer in 5 mm NMR tubes equipped with J. Young valves. Chemical shifts are given with respect to Me_4Si (^1H , ^{13}C), $\text{BF}_3 \cdot \text{OEt}_2$ (^{11}B) and H_3PO_4 (85%) (^{31}P).

Mass spectrometry: Mass spectra (ESI-MS) were recorded on a Bruker Daltonics micrOTOF instrument equipped with an Agilent 1100 series (LC) liquid chromatograph and direct infusion. The solid samples were dissolved in acetonitrile or water.

Crystal structure determinations: Single crystals suitable for X-ray diffraction were obtained by slow removal of the solvent from a saturated solution of $[\text{PPh}_4]_2[\text{B}_{12}(\text{CN})_{12}]$ in dimethyl sulfoxide. The single crystal X-ray diffraction study was performed on an Oxford Diffraction Gemini E Ultra diffractometer equipped with a $2\text{ K} \times 2\text{ K}$ EOS CCD area detector and a four-circle kappa goniometer using $\text{MoK}\alpha$ (0.71073 \AA) radiation at 150 K. The crystal was mounted onto a cryo loop using fluorinated oil and frozen in the cold nitrogen stream of the goniometer. Details of the crystallographic data collection and the refinement parameters can be found in Tables S1 and S2. The structures were solved by direct methods (SHELXT)³ using the program package OLEX2.⁴ Subsequent least-squares refinement on F^2 (SHELXL)⁵ located the positions of the remaining atoms in the electron density map. All non-hydrogen atoms were refined with anisotropic displacement parameters. Hydrogen atoms were placed in calculated positions using a riding model. The data were corrected for absorption.

Crystallographic data (excluding structure factors) for the structure reported in this paper has been deposited with the Cambridge Crystallographic Data Centre as supplementary publication no. CCDC-1979144. Copies of the data can be obtained free of charge on application to CCDC, 12 Union Road, Cambridge CB2 1EZ, UK [fax.: (internat.) + 44 1223/336-033; e-mail: deposit@ccdc.cam.ac.uk].

Table S1. Crystal data and structure refinement

CCDC number	1979144
Empirical formula	C _{59.56} H ₄₀ B ₁₂ I _{0.44} N _{11.57} P ₂
Formula weight	1164.58
Temperature/K	150(1)
Crystal system	monoclinic
Space group	<i>P</i> 2 ₁ /n
a/Å	14.8599(7)
b/Å	14.7377(6)
c/Å	15.2073(7)
α/°	90
β/°	109.961(6)
γ/°	90
Volume/Å ³	3130.3(3)
Z	2
ρ _{calc} g/cm ³	1.236
μ/mm ⁻¹	0.332
F(000)	1183.0
Crystal size/mm ³	0.33 × 0.19 × 0.05
Radiation	MoKα ($\lambda = 0.71073$)
2Θ range for data collection/°	5.472 to 58.784
Index ranges	-20 ≤ h ≤ 18, -20 ≤ k ≤ 17, -20 ≤ l ≤ 16
Reflections collected	17157
Independent reflections	7379 [R _{int} = 0.0213, R _{sigma} = 0.0299]
Data/restraints/parameters	7379/0/400
Goodness-of-fit on F ²	1.034
Final R indexes [I>=2σ (I)]	R ₁ = 0.0388, wR ₂ = 0.0932
Final R indexes [all data]	R ₁ = 0.0530, wR ₂ = 0.1011
Largest diff. peak/hole / e Å ⁻³	0.33/-0.35

Table S2. Fractional atomic coordinates ($\times 10^4$) and equivalent isotropic displacement parameters ($\text{\AA}^2 \times 10^3$). U_{eq} is defined as $1/3$ of the trace of the orthogonalised U_{II} tensor.

Atom	x	y	z	U(eq)
P1	8883.8(2)	4787.9(2)	2256.5(2)	16.63(9)
N5	6339.8(10)	7541.0(9)	4616.2(11)	36.1(3)
C7	9002.3(9)	3713.9(9)	2846.5(9)	18.3(3)
C8	8357.3(10)	3529.0(10)	3312.1(10)	23.4(3)
C19	7827.1(9)	4796.6(9)	1233.8(9)	18.6(3)
N1	3518.9(12)	6733.0(13)	2629.9(18)	50.0(5)
N4	5929.6(11)	5007.8(11)	2571.7(11)	41.7(4)
C30	7916.9(9)	6106.9(9)	2867.8(9)	22.0(3)
C25	8758.1(9)	5614.5(9)	3064.3(9)	18.2(3)
C12	9703.9(10)	3084.0(9)	2863.0(9)	21.9(3)
C11	9745.0(10)	2266.6(10)	3328.1(10)	25.5(3)
C20	7738.8(10)	5492.9(10)	589.3(9)	24.6(3)
C26	9485.1(10)	5707.9(10)	3930.5(10)	24.9(3)
N2	1913.6(19)	5168.1(14)	4419.4(15)	56.7(6)
C13	9890.9(9)	5040.9(10)	1909.2(9)	21.4(3)
C4	5722.7(11)	5025.7(10)	3215.1(11)	27.5(3)
C10	9095.8(10)	2080.5(10)	3771.4(10)	26.0(3)
C2	2708.9(19)	5105.8(16)	4544.0(16)	34.8(4)
C5	6019.4(10)	6872.1(10)	4718.7(10)	25.1(3)
C29	7797.9(10)	6691.2(10)	3534.5(10)	27.3(3)
C9	8406.0(10)	2708.7(10)	3770.6(10)	27.0(3)
C27	9356.5(11)	6295.1(10)	4583.0(10)	28.6(3)
C21	6920.1(11)	5549.9(11)	-194.1(10)	31.0(3)
C24	7094.7(10)	4173.7(10)	1096.4(10)	28.4(3)
C14	10409.7(10)	5835.9(10)	2199.1(11)	28.8(3)
C18	10118.8(11)	4450.1(11)	1298.9(11)	30.4(3)
C22	6192.8(11)	4926.5(12)	-329.9(10)	34.3(4)
C28	8513.5(11)	6778.4(10)	4389.9(10)	28.3(3)
C23	6276.0(11)	4245.1(12)	313.1(11)	37.0(4)
N6	3839.8(13)	7511.6(11)	5676.4(15)	59.2(5)
C6	4149.6(11)	6873.8(11)	5506.4(12)	34.1(4)
C17	10888.1(13)	4647.1(13)	1016.6(13)	40.9(4)
C16	11408.3(12)	5436.3(13)	1312.0(13)	41.7(4)
C15	11167.0(11)	6029.4(12)	1890.2(13)	37.4(4)
B5	5549.2(11)	5971.3(11)	4852.0(11)	21.0(3)
B2	3792.5(11)	5048.9(11)	4748.7(11)	22.1(3)
B4	5391.6(11)	5028.1(11)	4078.4(11)	21.9(3)
B6	4558.4(11)	5980.1(11)	5262.8(11)	22.5(3)
B3	4307.3(11)	4458.6(11)	4012.1(11)	23.0(3)

B1	4377.7(11)	5666.7(11)	4083.3(11)	22.3(3)
C1	3852.7(13)	6284.8(14)	3231.6(13)	30.5(4)
I1	3584.1(19)	6696(2)	3134(2)	30.5(4)
C3	3737(2)	3959.3(18)	3114.7(18)	35.5(3)
N3	3325(2)	3588(2)	2441(2)	54.1(7)
I3	3351.5(9)	3794.5(7)	2826.6(7)	35.5(3)
I2	2317(5)	5157(4)	4473(4)	34.8(4)

S 1.2 Synthesis of $[PPh_4]_2[B_{12}(CN)_{12}]$:

In a quartz tube 1.00 g (0.59 mmol) of $Na_2[B_{12}I_{12}]$ and 5.64 g (86.6 mmol, 147 eq.) NaCN was dissolved in 30 ml of water. The mixture was irradiated with UV light of a 150 W mercury medium pressure lamp (TQ 150 (Heraeus) obtained from UV-Technik) for 72 hours under intense stirring. The mixture was filtered in order to isolate the precipitate containing a large amount of $[B_{12}(CN)_{12}]^{2-}$ besides $[B_{12}(CN)_{11}I_1]^{2-}$ and $[B_{12}(CN)_{12}I_2]^{2-}$ (0.04 g of the crude product) as a tan solid (the filtrate was kept for the second fraction). The residue was resolved in hot water and $[PPh_4]Cl$ was added dropwise to the solution. The mixture was filtered and the white residue was washed with water (3×10 ml) and dried in vacuo. This yields 0.10 g of a mixture of $[PPh_4]_2[B_{12}(CN)_{12}]/[B_{12}(CN)_{11}I_1]/[B_{12}(CN)_{10}I_2]$ as a white solid as the first fraction. A second fraction was obtained by adding a solution of $[TBA]Br$ to the filtrate above in order to isolate $[TBA]_2[B_{12}(CN)_{12}]$ in a mixture with $[TBA]_2[B_{12}(CN)_{12-x}(OH)_x]$ ($x = 1, 2, 3$) and $[TBA]_2[B_{12}(CN)_{12-y}I_y]$ ($y = 1, 2$) as a tan solid (0.29 g).

$[PPh_4]_2[B_{12}(CN)_{12}]$: 1H NMR (400.13 MHz, CD_3CN , 298 K): $\delta = 2.14$ (s, H_2O), 7.73 (m, 32H, $[PPh_4]^+$), 7.94 (m, 8H, $[PPh_4]^+$). $^{11}B\{^1H\}$ NMR (128.38 MHz, CD_3CN): $\delta = -16.7$ (s, $[B_{12}(CN)_{11}I_1]^{2-}$), -17.8 (s, $[B_{12}(CN)_{11}I_1]^{2-}$), -18.2 (s, $[B_{12}(CN)_{12}]^{2-}$), -19.2 (s, $[B_{12}(CN)_{11}I_1]^{2-}$). ^{13}C NMR (100.62 MHz, CD_3CN , 298 K): $\delta = 131.3$ (d, $[PPh_4]^+$), 135.7 (d, $[PPh_4]^+$), 136.4 (s, $[PPh_4]^+$). ^{31}P NMR (161.97 MHz, CD_3CN , 298 K): $\delta = 22.9$ (s, $[PPh_4]^+$).

S 1.3 NMR spectroscopy:

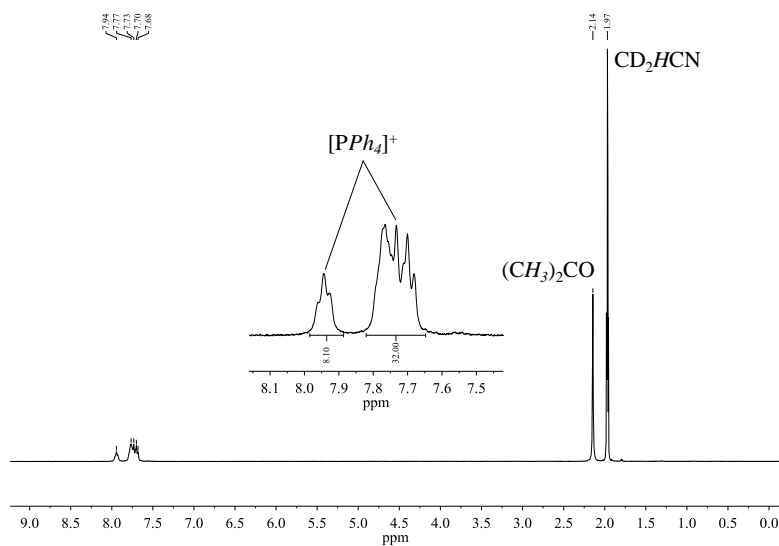


Figure S1. ¹H NMR spectrum (400.13 MHz, CD₃CN, 298 K) of [PPh₄]₂[B₁₂(CN)₁₂].

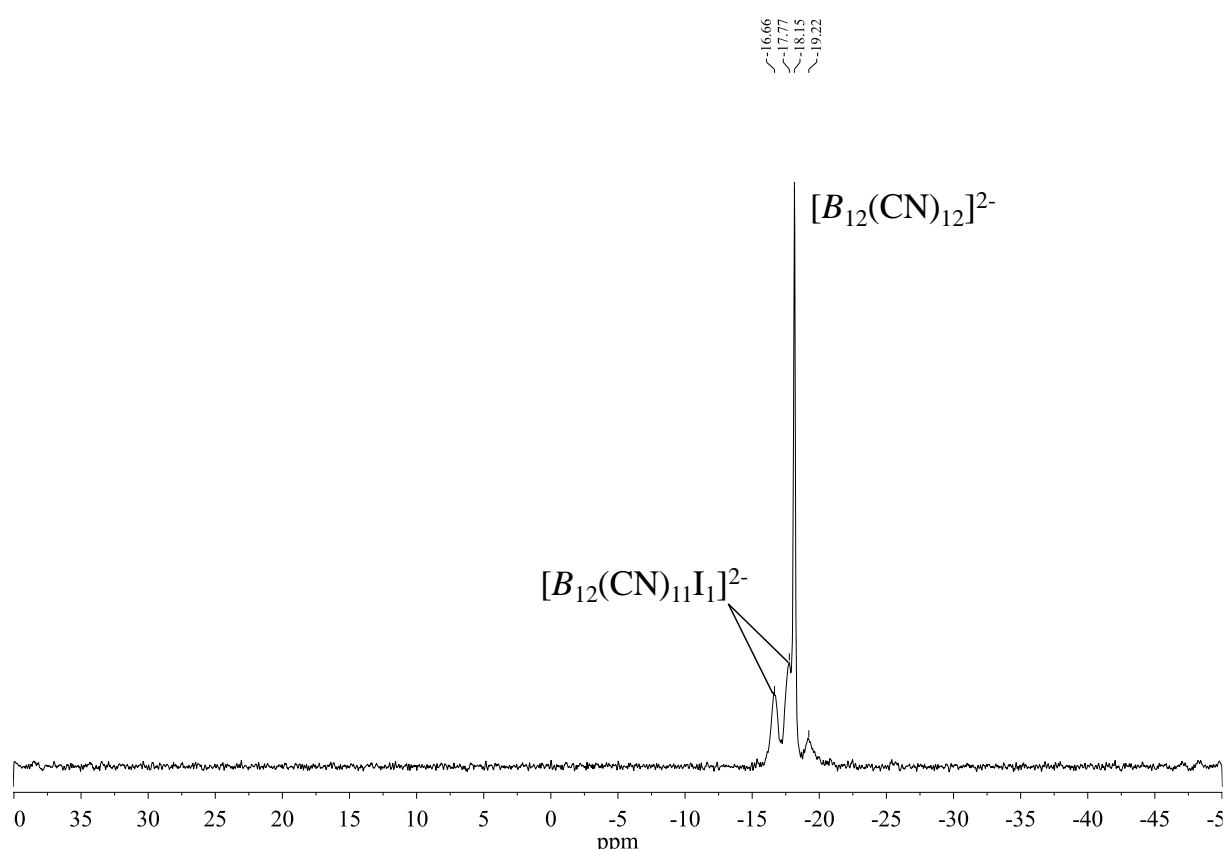


Figure S2. ¹¹B NMR spectrum (128.38 MHz, CD₃CN, 298 K) of [PPh₄]₂[B₁₂(CN)₁₂]/[B₁₂(CN)₁₁I].

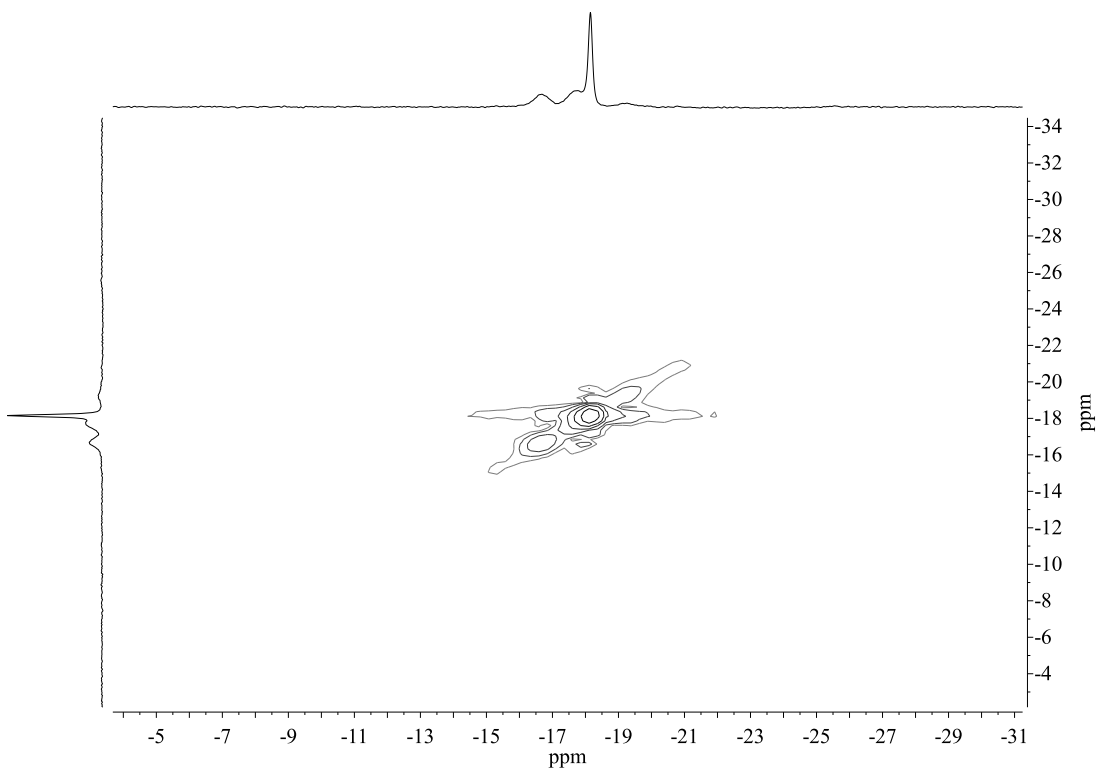


Figure S3. ^{11}B - ^{11}B COSY NMR spectrum (128.38 MHz, CD_3CN , 298 K) of $[\text{PPh}_4]_2[\text{B}_{12}(\text{CN})_{12}]$ / $[\text{B}_{12}(\text{CN})_{11}\text{I}]$.

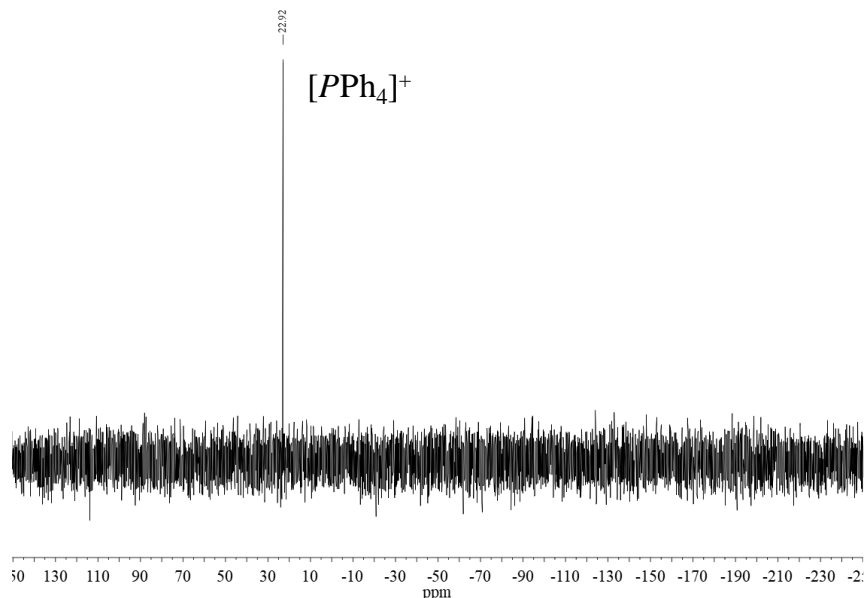


Figure S4. ^{31}P NMR spectrum (161.97 MHz, CD_3CN , 298 K) of $[\text{PPh}_4]_2[\text{B}_{12}(\text{CN})_{12}]$.

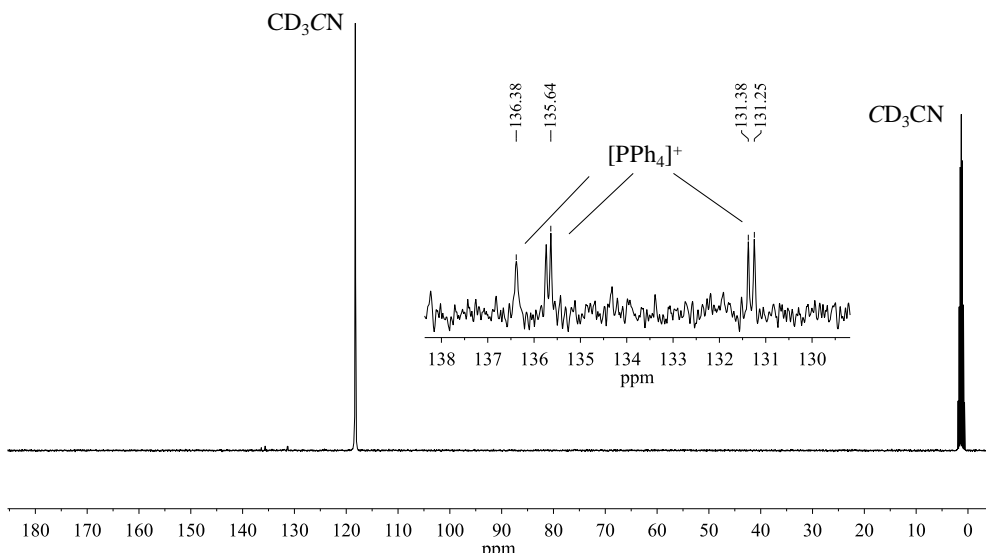


Figure S5. ^{13}C NMR spectrum (100.62 MHz, CD_3CN , 298 K) of $[\text{PPh}_4]_2[\text{B}_{12}(\text{CN})_{12}]$. The *ipso*-carbon atom of the $[\text{PPh}_4]^+$ is not observed due to the poor solubility of the salt.

The NMR spectra of $[\text{PPh}_4]_2[\text{B}_{12}(\text{CN})_{12}]$ clearly show the formation of the dodecacyano *closo*-dodecaborate. The ^1H , ^{13}C and ^{31}P NMR spectra (Figs. S1, S4, and S5) show the presence of the tetraphenylphosphonium cation. In the ^{11}B NMR spectrum (Fig. S2) the icosahedral $[\text{B}_{12}(\text{CN})_{12}]^{2-}$ is observed at a chemical shift of -18.2 ppm. This signal does not couple to other signals in the spectrum as evident from the ^{11}B - ^{11}B COSY spectrum (Fig. S3). Besides that, two signals with approximate equal intensity at -16.7 and -17.8 ppm are observed, which represent the two independent five-membered rings in the $[\text{B}_{12}(\text{CN})_{11}\text{I}_1]^{2-}$ anion, which is the major impurity in the product. The small singlet at -19.2 ppm shows a cross-peak to the signal at 18.8 ppm and can be assigned to either the iodine-bonded or the antipodal boron atom in $[\text{B}_{12}(\text{CN})_{10}\text{I}_2]^{2-}$.

S 1.4 Vibrational spectroscopy:

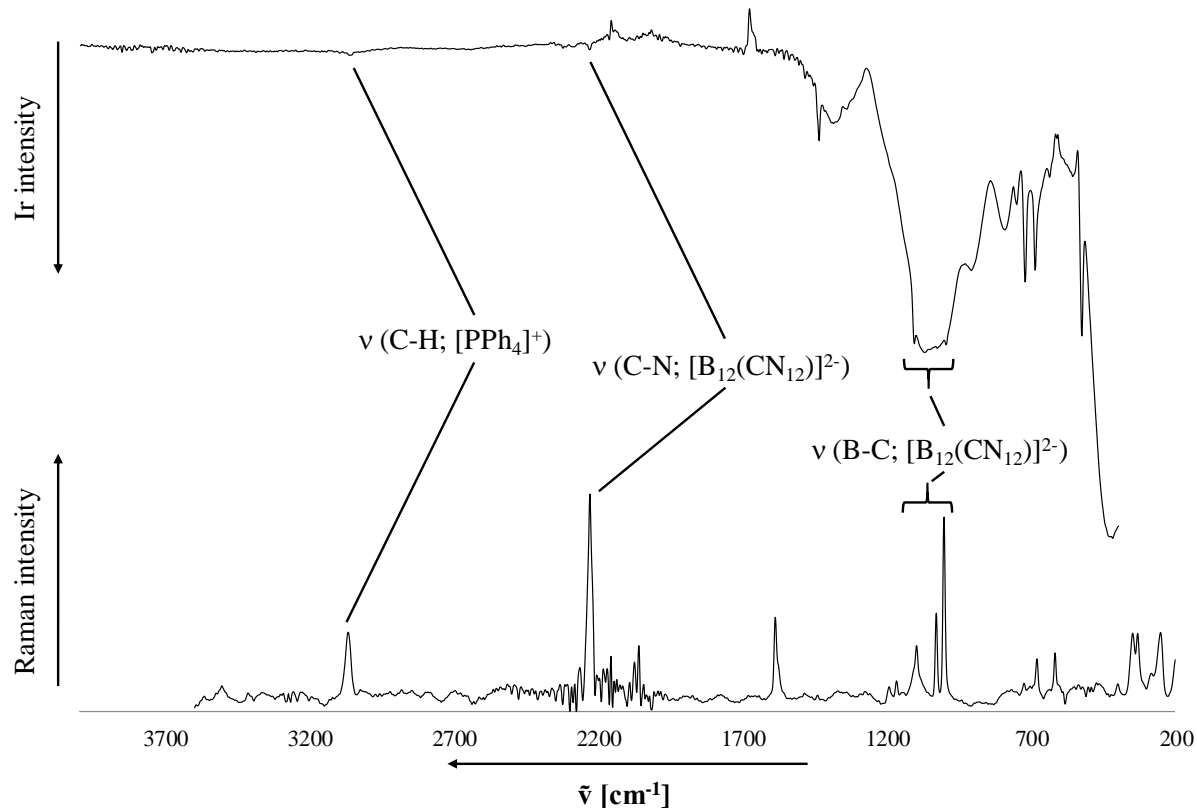


Figure S6. IR (diamond ATR, top) and Raman spectrum (100 mw, 10000 Scans, bottom) of $[\text{PPh}_4]_2[\text{B}_{12}(\text{CN})_{12}]$.

FT-IR and FT-Raman spectra (Fig. S6) show the expected signals for the $[\text{B}_{12}(\text{CN})_{12}]^{2-}$ anion. While the infrared spectrum only shows a very weak band at 2232 cm^{-1} for the symmetry forbidden C≡N stretching mode, this vibration becomes very strong in the Raman spectrum at 2230 (calc. 2335 cm^{-1} at the B3LYP/def2-TZVPP level) proving the presence of the free $[\text{B}_{12}(\text{CN})_{12}]^{2-}$ anion. Furthermore, the asymmetric B-C vibrations can be seen in the range of $1107\text{-}1071 \text{ cm}^{-1}$ demonstrating the formed boron-carbon bonds. Additional signals could be assigned to the tetraphenylphosphonium cation by comparing with measured spectra of $[\text{PPh}_4]\text{Cl}$. Tables S3 and S4 compile the obtained signals in comparison to calculated data for $[\text{B}_{12}(\text{CN})_{12}]^{2-}$ and $[\text{B}_{12}(\text{CN})_{11}\text{I}_1]^{2-}$.

Table S3. IR frequencies (in cm^{-1}) of experimental and calculated (B3LYP/def2-TZVPPP) spectra of $[\text{PPh}_4]_2[\text{B}_{12}(\text{CN})_{12}]$ and $[\text{PPh}_4]_2[\text{B}_{12}(\text{CN})_{11}\text{I}_1]^2$ with assignment. Calculated relative intensities are given in brackets.

$\tilde{\nu}$ exp.	$\tilde{\nu}$ calc. $[\text{B}_{12}(\text{CN})_{12}]^{2-}$	$\tilde{\nu}$ calc. $[\text{B}_{12}(\text{CN})_{11}\text{I}_1]^{2-}$	Assignment
3065 (vw)			$[\text{PPh}_4]^+$
2232 (vw)	2336 (0) 2335 (0)	2335 (0)	ν (C-N)
1437 (m)			$[\text{PPh}_4]^+$
1387 (m)			
1341 (w)			$[\text{PPh}_4]^+$
1107 (s)	1116 (100)	1102 (5) 1112 (61)	ν (B-C)
1071 (s)		1114(100) 1089 (0.3) 1083 (1)	$+ [\text{PPh}_4]^+$
997 (m)			$[\text{PPh}_4]^+$
909 (sh, m)		894	ν (B-I)
793 (m)			
752 (w)			
723 (m)			$[\text{PPh}_4]^+$
688 (m)			$[\text{PPh}_4]^+$
638 (vw)	650 (28)	654 (14) 636 (19)	δ (B-C)
613 (vw)		604 (48)	
558 (w)		580 (1)	δ (B-I)
526 (s)			$[\text{PPh}_4]^+$
419 (vs)	382 (15)	389 (9) 380 (15) 378 (5)	δ (C-N)

Table S4. Raman frequencies (in cm^{-1}) of experimental and calculated (B3LYP/def2-TZVPPP) spectra of $[\text{PPh}_4]_2[\text{B}_{12}(\text{CN})_{12}]$ with assignment. Calculated relative Raman activities are given in brackets.

$\tilde{\nu}$ exp.	$\tilde{\nu}$ calc. $[\text{B}_{12}(\text{CN})_{12}]^{2-}$	$\tilde{\nu}$ calc. $[\text{B}_{12}(\text{CN})_{11}\text{I}_1]^{2-}$	Assignment
3068 (w)			$[\text{PPh}_4]^+$
2230 (m)	2335 (100) 2336 (18)	2334 (1391) 2335 (18)	ν (C-N)
1587 (w)			$[\text{PPh}_4]^+$
1096 (vw)	1091 (1)	1114 (2)	
1028 (w)	1107 (3)	1112 (6) 1103 (6)	ν (B-C) + $[\text{PPh}_4]^+$
1002 (m)		1089 (13) 1083 (0)	
		894 (10)	ν (B-I)
	746 (1)	787 (2) 780 (5) 762 (1) 745 (1) 737 (5) 717 (12)	ν (B-B) + δ (B-C)
679 (vw)			$[\text{PPh}_4]^+$
	650 (2)	654 (0) 652 (0) 636 (2)	δ (B-C)
617 (vw)		604 (6)	
		579 (1)	δ (B-I)
	423 (0)	424 (0) 423 (0)	δ (C-N)
	382 (0)	389 (0) 380 (0)	δ (C-N)
348 (w)	348 (4) 324 (1)	355 (1) 341 (1) 324 (0)	δ (B-B)
251 (vw)			
199 (vw)		181 (0)	

S 1.5 Mass spectrometry:

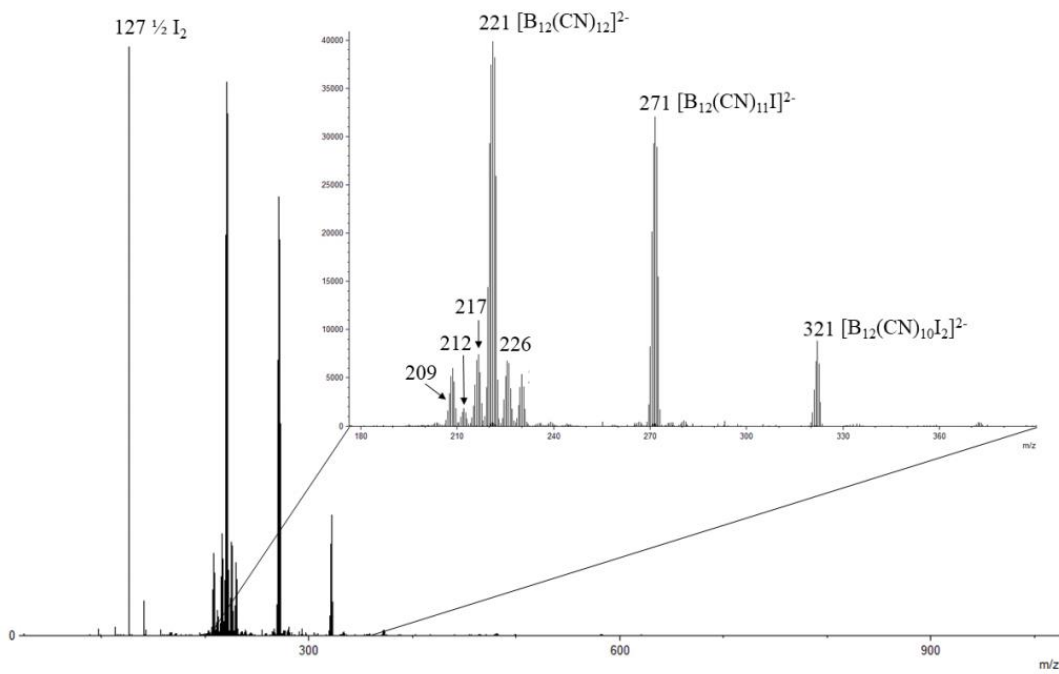


Figure S7. Mass spectrum (ESI, neg. mode) of the first fraction. [m/z]: 127 $\frac{1}{2}$ I_2^- , 212 $[B_{12}(CN)_{10}(OH)_2]^{2-}$, 217 $[B_{12}(CN)_{11}(OH)]^{2-}$, 221 $[B_{12}(CN)_{12}]^{2-}$, 226 $[B_{12}(CN)_{11}Cl]^{2-}$, 271 $[B_{12}(CN)_{11}I]^{2-}$, 321 $[B_{12}(CN)_{10}I_2]^{2-}$.

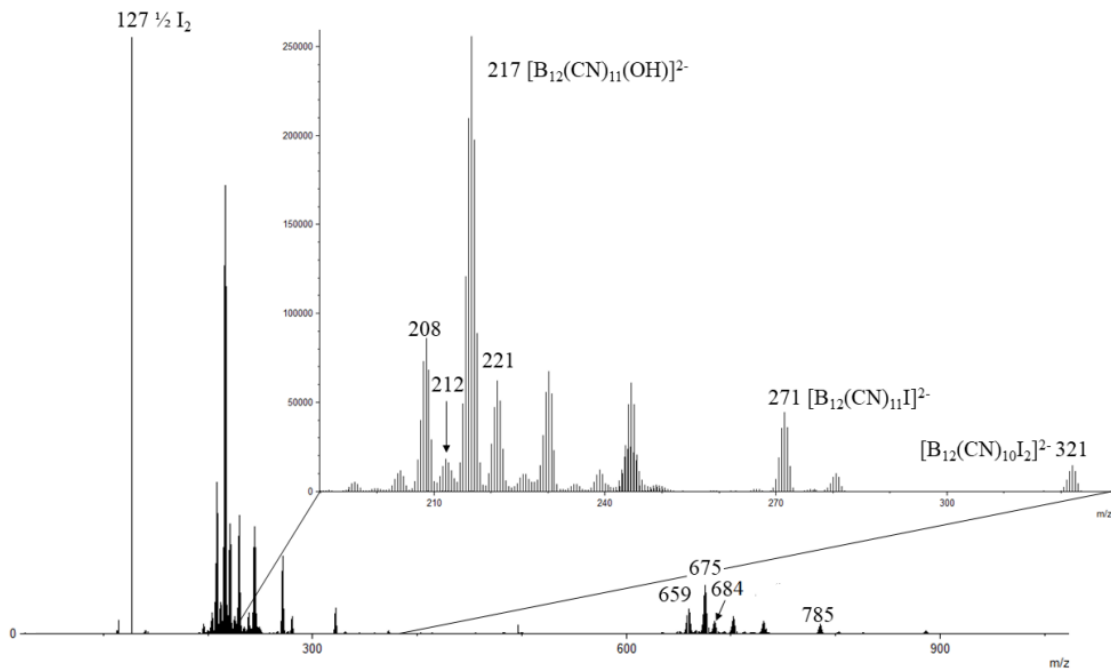


Figure S8. Mass spectrum (ESI, neg. mode) of the second fraction. 127 $\frac{1}{2}$ I_2^- , 208 $[B_{12}(CN)_9(OH)_3]^{2-}$, 212 $[B_{12}(CN)_{10}(OH)_2]^{2-}$, 217 $[B_{12}(CN)_{11}(OH)]^{2-}$, 221 $[B_{12}(CN)_{12}]^{2-}$, 271 $[B_{12}(CN)_{11}I]^{2-}$, 321 $[B_{12}(CN)_{10}I_2]^{2-}$, 659 $[NBu_4][B_{12}(CN)_9(OH)_3]^-$, 675 $[NBu_4][B_{12}(CN)_{11}(OH)]^-$, 684 $[NBu_4][B_{12}(CN)_{12}]^-$, 785 $[NBu_4][B_{12}(CN)_{11}I]^-$.

S 1.6 Crystal structure of $[\text{PPh}_4]_2[\text{B}_{12}(\text{CN})_{11.5}\text{I}_{0.5}]$

Single crystals were generated by slow evaporation of a saturated solution of $[\text{PPh}_4]_2[\text{B}_{12}(\text{CN})_{12}]$ in dimethyl sulfoxide at room temperature over three weeks.

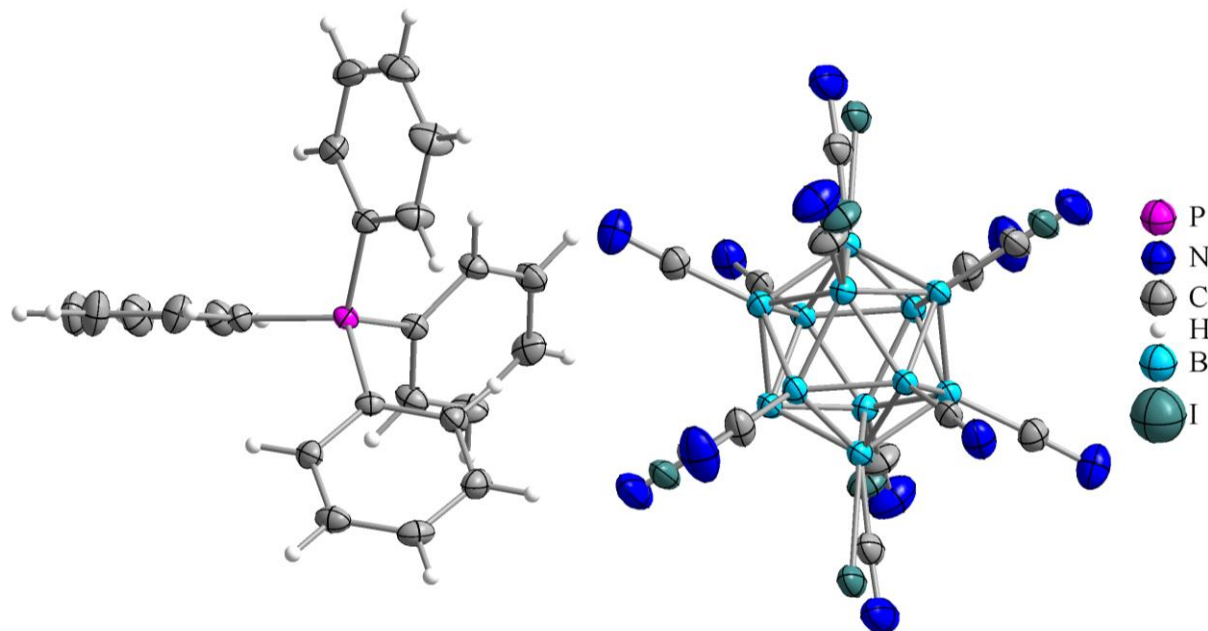


Figure S9. Part of the crystal structure of $[\text{PPh}_4]_2[\text{B}_{12}(\text{CN})_{11.5}\text{I}_{0.5}]$. Thermal ellipsoids are drawn with 50% probability.

The salt $[\text{PPh}_4]_2[\text{B}_{12}(\text{CN})_{12}]$ crystallizes together with $[\text{B}_{12}(\text{CN})_{11}\text{I}_1]^{2-}$ solvent-free in the monoclinic crystal system in space group $P2_1/c$. The anion to cation ratio is 1 : 2. The impurity of $[\text{B}_{12}(\text{CN})_{11}\text{I}_1]^{2-}$ co-crystallizes with the $[\text{B}_{12}(\text{CN})_{12}]^{2-}$ anion. Both anions possess nearly equal volumes and electronic properties. Therefore, the structure was refined as a solid solution with partial occupancy of iodine atoms and cyanide groups in six of the twelve positions resulting in a molecular composition of $[\text{PPh}_4]_2[\text{B}_{12}(\text{CN})_{11.5}\text{I}_{0.5}]$. The bond lengths of the $[\text{B}_{12}(\text{CN})_{12}]^{2-}$ anion compared to other cyanoborates are compiled in Tab. S5.

Table S5. Comparison of the bond lengths (in pm) of the $[B_{12}(CN)_{12}]^{2-}$ anion with typical salts of $[B(CN)_4]^-$.

Compound	distance (B-C)	distance (C-N)
$[PPh_4]_2[B_{12}(CN)_{12}]$	152.7(3)	110.0(3)
	154.6(2)	111.5(2)
	154.8(2)	112.2(2)
	155.1(2)	113.5(4)
$K[B(CN)_4]^6$	155.8(2)	113.8(4)
	159.5(1)	114.2(1)
	158.9(2)	113.1(3)
	158.2(3)	113.5(3)
$[Bu_4N][B(CN)_4]^6$	159.0(3)	114.1(3)
	158.9(2)	114.2(3)
	158.9(4)	112.5(4)
$Na[B(CN)_4] \cdot THF^7$	158.8(4)	114.2(4)
	159.2(2)	113.3(2)

^aCalculated values (B3LYP/def2-TZVPP) are given in *italics*.

The boron-carbon as well as the carbon-nitrogen bonds are slightly shorter than those in the related tetracyano borates. This indicates stronger bonds in the *closo*-dodecaborate $[B_{12}(CN)_{12}]^{2-}$ compared to the smaller borates and underlines the stability of this anion.

S 2 Details theoretical determination of Ne and He attachment enthalpies to [B₁₂(CN)₁₁]⁻

The 0K attachment enthalpies were determined by calculating the basis set superposition error (BSSE) and Zero Point Energy (ZPE) corrected difference in electronic energies between the reagents ([B₁₂(CN)₁₁ + Ng]⁻ and the product [B₁₂(CN)₁₁Ng]⁻, Ng=He, Ne. Gaussian09⁸ and NWChem⁹ were used for the calculations. Previous theoretical investigations on the similar system [B₁₂(CN)₁₁Ar]⁻ have shown that dispersion corrected DFT methods and spin-component scaled MP2 (SCS-MP2) with large basis sets gave very similar results within a few kJ/mol and are also similar to CCSD(T) energies.¹⁰

Using dispersion corrected B3LYP/def2-tzvppd,¹¹ we calculated [B₁₂(CN)₁₁He]⁻ to be 9 kJ/mol more favorable than the separated reagents. However, ZPE correction using the harmonic approximation is calculated to lower this value by around 6 kJ/mol (resulting in a ZPE corrected attachment energy of 3 kJ/mol). The SCS-MP2¹² basis set limit approach suggests an attachment energy of 3.4 kJ/mol (see Figure S10) which lies considerably below the DFT ZPE correction. A substantial error bar should be considered for the large value of ZPE correction, since the “flat” B—He potential is likely not well described by the harmonic oscillator. Anharmonic frequency analysis for the DFT and SCS-MP2 with large basis sets is not feasible for us, making it difficult to decide if the [B₁₂(CN)₁₁He]⁻ is very slightly bound or actually unbound.

The same DFT method predicts [B₁₂(CN)₁₁Ne]⁻ to be 12 kJ/mol more favorable than the separated reagents. ZPE corrections are calculated to be around 3kJ/mol. This results in 0K Enthalpies of around 9 kJ/mol. This result is confirmed by using different DFT functionals and basis sets, see Table S7. The SCS-MP2 basis set limit approach suggests an attachment energy of 7.5 kJ/mol (see Figure S11). Therefore, we conclude that [B₁₂(CN)₁₁Ne]⁻ is a thermodynamically stable minimum and the ion should be observable at low temperatures.

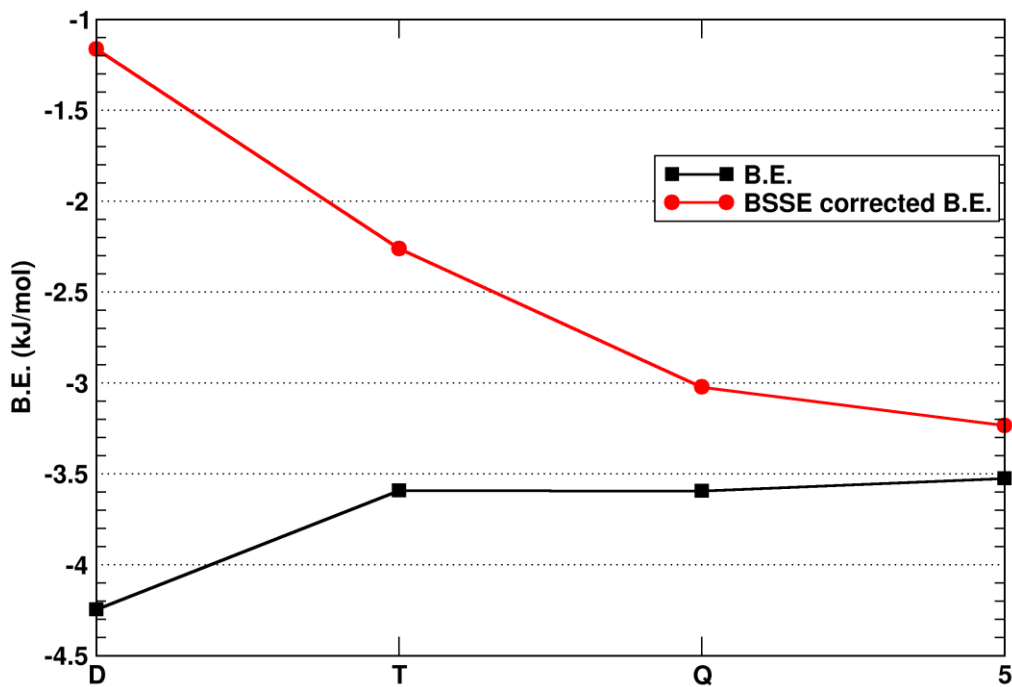


Figure S10. Convergence of the calculated energy for SCS-MP2 with and without BSSE correction, by approaching the basis set limit for the case of He binding to $[B_{12}(CN)_{11}]^-$. The x-axis represents the basis sets of increasing size (from cc-pVDZ to cc-pV5Z)¹³

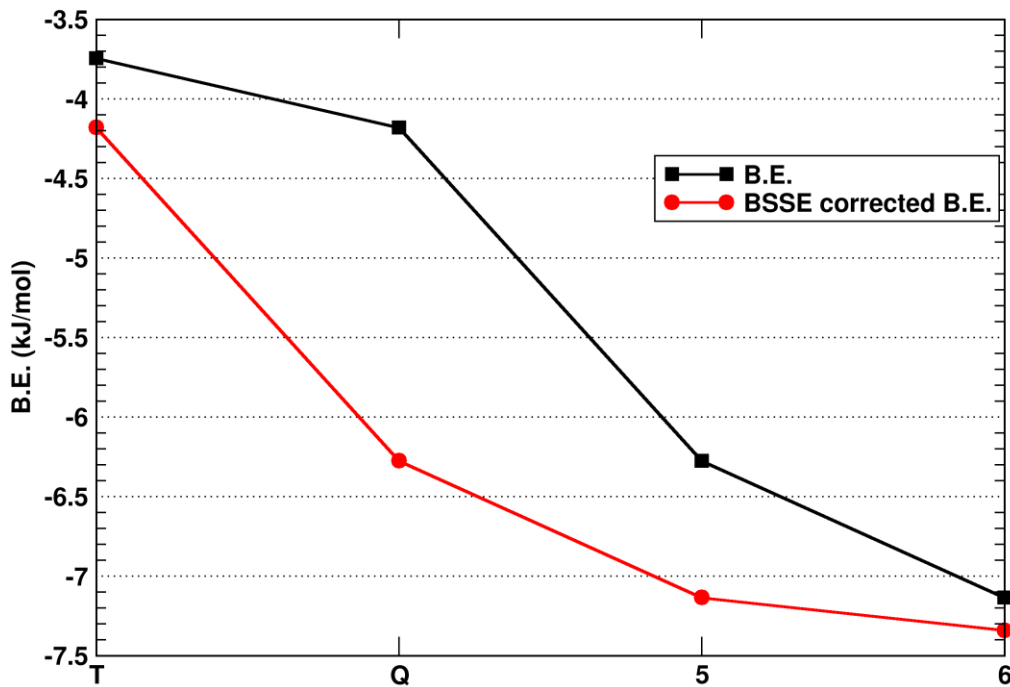


Figure S11. Convergence of the calculated energy for SCS-MP2 with and without BSSE correction, by approaching the basis set limit for the case of Ne binding to $[B_{12}(CN)_{11}]^-$. The x-axis represents the basis sets of increasing size (from cc-pVTZ to cc-pV6Z)

Table S6. Results of Ne attachment enthalpy (in kJ/mol) evaluation for $[B_{12}(CN)_{11}Ne]^-$ different DFT functionals and basis set sizes.

Level of theory	Ne attachment enthalpy (0 K)
B3LYP-GD3BJ/def2-TZVPP	-8.0
B3LYP-GD3BJ/def2-QZVPP	-8.9
PBE1PBE-GD3BJ/def2-TZVPP	-9.7
PBE1PBE-GD3BJ/def2-QZVPP	-10.6

S 3 Ion molecule reactions of $[B_{12}(CN)_{11}]^-$ with He and Ne

S 3.1 Experimental details

Ion molecule reactions were performed by using the Leipzig cryogenic ion trap triple mass spectrometer described in detail elsewhere.¹⁴ In brief, $[B_{12}(CN)_{11}]^-$ anions were produced via skimmer collision induced dissociation (sCID) from precursor ions formed using a nanospray ion-source with a 0.1 mmol/l solution of $[B_{12}(CN)_{12-n}(OH)_n][N(C_4H_9)_4]_2$ ($n= 0\text{--}5$) in CH_3OH/H_2O (2:1, v/v). The ions were thermalized (close to room temperature) in a radio-frequency (RF) ion guide filled with helium buffer gas, selected according to their m/z ratios in a quadrupole mass filter, deflected by 90° and subsequently trapped in a temperature-controllable RF ring-electrode ion-trap. The ion trap was filled with either helium ($2.0 \cdot 10^{-3}$ mbar) or a 10% mixture of neon in helium ($2.0 \cdot 10^{-3}$ mbar) at various temperatures in order to form $[B_{12}(CN)_{11}Ne]^-$ complexes via three-body collisions.¹⁵ Every 100 ms all ions were extracted from the ion trap and focused into the center of the extraction region of an orthogonally mounted reflectron TOF tandem mass spectrometer. TOF mass spectra were recorded by averaging over 2000 extraction cycles.

S 3.2 TOF mass spectra $[B_{12}(CN)_{11}Ne]^-$

Figure S12 shows time-of-flight mass spectra of $[B_{12}(CN)_{11}]^-$ trapped with the collision gases helium and a mixture of 10% neon in helium. Due to the significant natural abundance of two boron isotopes (80% ^{11}B , 20% ^{10}B) an isotopologue distribution is observed for $[B_{12}(CN)_{11}]^-$ in the mass spectra. The signal-to-noise ratio of $[B_{12}(CN)_{11}Ne]^-$ drops below 3:1 at 50 K (Figure S1 a). Because N₂ is a common contaminant in our ion trap, a $[B_{12}(CN)_{11}N_2]^-$ signal is observed from 45 K on, where N₂ is gaseous using our standard experimental settings.

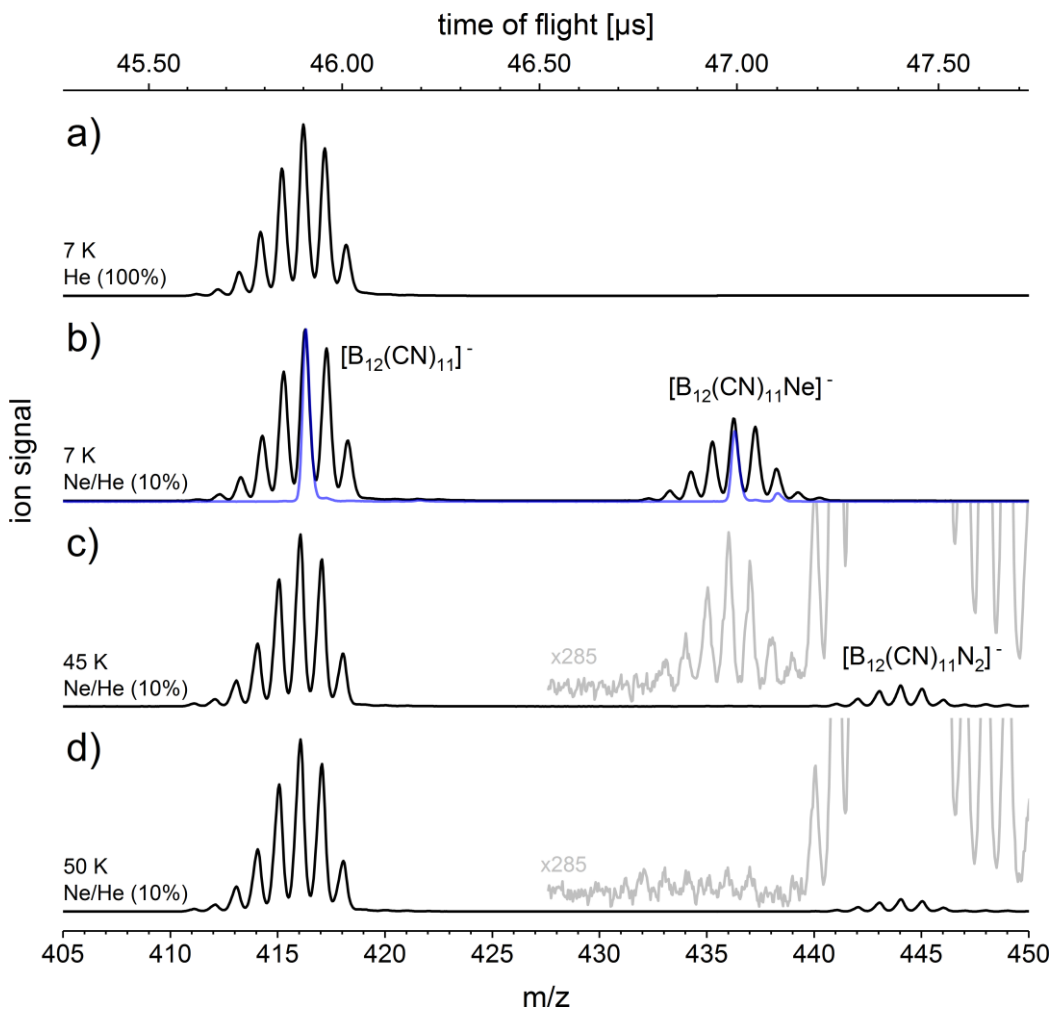


Figure S12. Time-of-flight mass spectra of $[B_{12}(CN)_{11}]^-$, trapped at constant pressure ($2.0 \cdot 10^{-3}$ mbar) with the collision gas helium at 7 K (a) and a 10% mixture of neon in helium at 7 K (b), 45 K (c) and 50 K (d). The isotopologue distribution (black trace) and the most intense mass signal at $m/z = 416$ (blue trace) were mass-selected.

S 4 Energy decomposition analysis

S 4.1 Method details

Energy decomposition analysis (EDA) was carried out using the Amsterdam Density Functional (ADF) software package (version r60451 from 2017).¹⁶ Structures obtained by Gaussian09 geometry relaxation on B3LYP-GD3BJ/def2-QZVPP level of theory were imported and subjected to a geometry optimization using the B3LYP-D3BJ/AUG/ATZP model chemistry as implemented in ADF. The resulting structures were analyzed with respect to energy

decomposition of the fragments separated by the B-Ng (Ng = He,Ne) bond in terms of the Morokuma-Ziegler EDA scheme as summarized by Bickelhaupt and Baerends.¹⁷ Due to the dative character of the B-Ng bonds of all species, a heterolytical separation scheme was applied and the full charge was assigned to the ion instead of the Ng atom. Note that in contrast to most of the common quantum chemical software, ADF employs Slater-type functions in the standard basis sets.

S 4.2 Bond parameters of the B-Ne bond in Na[B₁₂(CN)₁₁Ne]

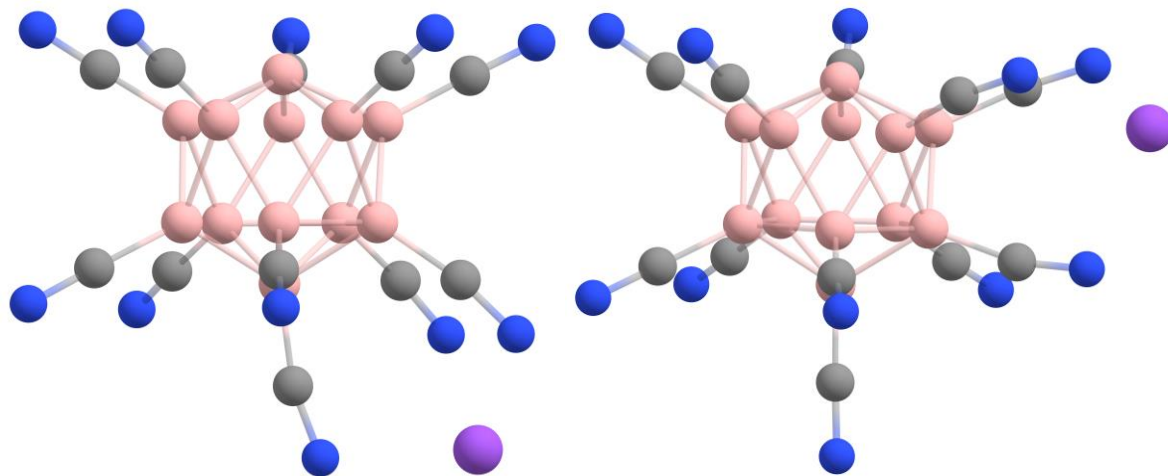


Figure S13. Calculated isomers for Na[B₁₂(CN)₁₁] on B3LYP-GD3BJ/def2-TZVPP level of theory. The left isomer is about 22 kJ/mol lower in energy and was therefore considered for further attachment reactions.

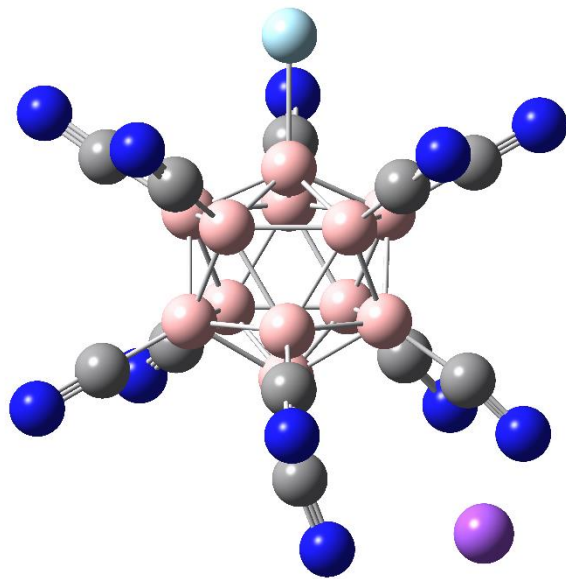


Figure S14. Calculated minimum structure for $\text{Na}[\text{B}_{12}(\text{CN})_{11}\text{Ne}]$ on B3LYP-GD3BJ/def2-TZVPP level of theory.

Table S7. Results of Ne attachment enthalpy evaluation and bonding analysis of the B-Ne bonds at the bcp (B3LYP-GD3BJ/def2-TZVPP).

Ion	$[\text{B}_{12}(\text{CN})_{11}\text{Ne}]^-$	$\text{Na}[\text{B}_{12}(\text{CN})_{11}\text{Ne}]$
Ne attachment enthalpy (0 K), kJ/mol	-7.954	-11.931
Bond length, Å	2.093	1.990
$\rho_{\text{bcp}}, e \cdot \text{\AA}^{-3}$	0.158	0.192
$H_{\text{bcp}}/\rho_{\text{bcp}}, \text{Ha} \cdot e^{-1}$	-0.159	-0.279
δ	0.146	0.177
Q_{NPA} bound Ng, e	+0.100	+0.125

S 5 Cartesian coordinates of all optimized geometries

Table S8. Cartesian coordinates of the optimized geometry of $[B_{12}(CN)_{11}Ne]^+$ (C_{5v}) obtained at the B3LYP-GD3BJ/def2-QZVPP level

Tag	Symbol	X	Y	Z
1	B	1.089110000	1.073383000	0.738510000
2	B	-1.105425000	-1.089262000	-0.778339000
3	B	-0.002665000	0.001620000	1.660513000
4	B	-0.684231000	1.369077000	0.734371000
5	B	0.257061000	1.529802000	-0.779353000
6	B	1.536200000	0.229144000	-0.775532000
7	B	1.355826000	-0.704737000	0.740355000
8	B	-0.253033000	-1.507509000	0.738265000
9	B	0.694160000	-1.389123000	-0.775944000
10	B	0.002440000	-0.001594000	-1.495002000
11	B	-1.375808000	0.715143000	-0.780828000
12	B	-1.513673000	-0.225707000	0.735537000
13	C	2.570398000	-1.337034000	1.410883000
14	C	2.836689000	0.422944000	-1.543509000
15	C	2.065112000	2.034532000	1.408114000
16	C	0.474795000	2.825236000	-1.549458000
17	C	-1.296892000	2.595705000	1.401247000
18	C	-2.540164000	1.320975000	-1.552754000
19	C	-2.869667000	-0.427830000	1.402772000
20	C	-2.041307000	-2.010967000	-1.548523000
21	C	-0.479995000	-2.858604000	1.407605000
22	C	1.281974000	-2.565493000	-1.543675000
23	C	-0.004843000	0.002645000	3.186369000
24	N	-3.401708000	1.769529000	-2.166869000
25	N	0.636193000	3.784111000	-2.161917000
26	N	2.805156000	2.762756000	1.900762000
27	N	3.798716000	0.566405000	-2.155490000
28	N	1.717053000	-3.435633000	-2.155352000

29	N	-0.652089000	-3.882896000	1.899416000
30	N	-0.006662000	0.003014000	4.335327000
31	N	-1.761151000	3.525435000	1.891890000
32	N	3.491135000	-1.816350000	1.904018000
33	N	-3.897579000	-0.581100000	1.893251000
34	N	-2.733906000	-2.692806000	-2.161702000
35	Ne	0.005749000	-0.003109000	-3.585054000

Table S9. Cartesian coordinates of the optimized geometry of [B₁₂(CN)₁₁Ne] (*C*_{5v}) obtained at the SCS-MP2 cc-pVQZ level

Tag	Symbol	X	Y	Z
1	B	1.53289553	0.00000000	0.73809576
2	B	-1.56020563	0.00000000	-0.78033802
3	B	-0.00000000	0.00000000	1.66374335
4	B	0.47369077	1.45787029	0.73809576
5	B	1.26223287	0.91706586	-0.78033802
6	B	1.26223287	-0.91706586	-0.78033802
7	B	0.47369077	-1.45787029	0.73809576
8	B	-1.24013854	-0.90101339	0.73809576
9	B	-0.48213005	-1.48384373	-0.78033802
10	B	-0.00000000	0.00000000	-1.49815311
11	B	-0.48213005	1.48384373	-0.78033802
12	B	-1.24013854	0.90101339	0.73809576
13	C	0.89877325	-2.76613963	1.41007517
14	C	2.33135561	-1.69382900	-1.54823555
15	C	2.90849133	0.00000000	1.41007517
16	C	2.33135561	1.69382900	-1.54823555
17	C	0.89877325	2.76613963	1.41007517
18	C	-0.89049860	2.74067289	-1.54823555
19	C	-2.35301891	1.70956831	1.41007517
20	C	-2.88171401	0.00000000	-1.54823555
21	C	-2.35301891	-1.70956831	1.41007517

22	C	-0.89049860	-2.74067289	-1.54823555
23	C	-0.00000000	0.00000000	3.19526310
24	N	-1.19719357	3.68458296	-2.16436913
25	N	3.13429347	2.27719750	-2.16436913
26	N	3.96382847	0.00000000	1.91138360
27	N	3.13429347	-2.27719750	-2.16436913
28	N	-1.19719357	-3.68458296	-2.16436913
29	N	-3.20680459	-2.32987992	1.91138360
30	N	-0.00000000	0.00000000	4.36344768
31	N	1.22489036	3.76982489	1.91138360
32	N	1.22489036	-3.76982489	1.91138360
33	N	-3.20680459	2.32987992	1.91138360
34	N	-3.87419979	-0.00000000	-2.16436913
35	Ne	0.00000000	0.00000000	-3.62696573

Table S10. Cartesian coordinates of the optimized geometry of $[B_{12}(CN)_{12}]^{2-}$ (point group: I_h), obtained at the B3LYP/def2-TZVPP level.

Tag	Symbol	X	Y	Z
1	B	0.000000000000	0.000000000000	1.705355000000
2	B	1.450661000000	0.471348000000	0.762658000000
3	B	1.450661000000	0.471348000000	0.762658000000
4	B	0.000000000000	1.525316000000	0.762658000000
5	B	0.896558000000	1.234006000000	0.762658000000
6	B	0.000000000000	1.525316000000	0.762658000000
7	B	0.896558000000	1.234006000000	0.762658000000
8	B	0.000000000000	0.000000000000	1.705355000000
9	B	1.450661000000	0.471348000000	0.762658000000
10	B	1.450661000000	0.471348000000	0.762658000000
11	B	0.896558000000	1.234006000000	0.762658000000
12	B	0.896558000000	1.234006000000	0.762658000000
13	C	2.759582000000	0.896642000000	1.450798000000
14	C	1.705515000000	2.347440000000	1.450798000000
15	C	0.000000000000	2.901596000000	1.450798000000

16	C	2.759582000000	0.896642000000	1.450798000000
17	C	1.705515000000	2.347440000000	1.450798000000
18	C	0.000000000000	0.000000000000	3.244083000000
19	C	2.759582000000	0.896642000000	1.450798000000
20	C	0.000000000000	0.000000000000	3.244083000000
21	C	1.705515000000	2.347440000000	1.450798000000
22	C	1.705515000000	2.347440000000	1.450798000000
23	C	0.000000000000	2.901596000000	1.450798000000
24	C	2.759582000000	0.896642000000	1.450798000000
25	N	0.000000000000	3.931412000000	1.965706000000
26	N	3.738995000000	1.214873000000	1.965706000000
27	N	2.310826000000	3.180579000000	1.965706000000
28	N	2.310826000000	3.180579000000	1.965706000000
29	N	3.738995000000	1.214873000000	1.965706000000
30	N	0.000000000000	0.000000000000	4.395452000000
31	N	3.738995000000	1.214873000000	1.965706000000
32	N	2.310826000000	3.180579000000	1.965706000000
33	N	0.000000000000	3.931412000000	1.965706000000
34	N	0.000000000000	0.000000000000	4.395452000000
35	N	2.310826000000	3.180579000000	1.965706000000
36	N	3.738995000000	1.214873000000	1.965706000000

Table S11. Cartesian coordinates of the optimized geometry of $[B_{12}(CN)_{11}I]^{2-}$ (point group: C_{5v}), obtained at the B3LYP/def2-TZVPP level.

Tag	Symbol	X	Y	Z
1	B	0.895928000000	1.233140000000	1.370335000000
2	B	0.000000000000	1.523179000000	0.157938000000
3	B	1.448629000000	0.470688000000	0.157938000000
4	B	1.449642000000	0.471017000000	1.370335000000
5	B	0.000000000000	0.000000000000	2.314196000000
6	B	1.448629000000	0.470688000000	0.157938000000
7	B	0.000000000000	0.000000000000	1.108022000000

8	B	0.895302000000	1.232278000000	0.157938000000
9	B	0.000000000000	1.524244000000	1.370335000000
10	B	1.449642000000	0.471017000000	1.370335000000
11	B	0.895302000000	1.232278000000	0.157938000000
12	B	0.895928000000	1.233140000000	1.370335000000
13	C	2.763375000000	0.897875000000	0.835259000000
14	C	1.705364000000	2.347232000000	2.057273000000
15	C	2.759337000000	0.896563000000	2.057273000000
16	C	0.000000000000	2.901338000000	2.057273000000
17	C	0.000000000000	0.000000000000	3.852832000000
18	C	1.705364000000	2.347232000000	2.057273000000
19	C	0.000000000000	2.905585000000	0.835259000000
20	C	1.707860000000	2.350667000000	0.835259000000
21	C	1.707860000000	2.350667000000	0.835259000000
22	C	2.763375000000	0.897875000000	0.835259000000
23	C	2.759337000000	0.896563000000	2.057273000000
24	N	3.747379000000	1.217597000000	1.340593000000
25	N	3.739499000000	1.215037000000	2.570771000000
26	N	2.316008000000	3.187711000000	1.340593000000
27	N	0.000000000000	3.931941000000	2.570771000000
28	N	2.311137000000	3.181007000000	2.570771000000
29	N	0.000000000000	3.940227000000	1.340593000000
30	N	2.311137000000	3.181007000000	2.570771000000
31	N	3.739499000000	1.215037000000	2.570771000000
32	N	2.316008000000	3.187711000000	1.340593000000
33	N	0.000000000000	0.000000000000	5.004270000000
34	N	3.747379000000	1.217597000000	1.340593000000
35	I	0.000000000000	0.000000000000	3.286875000000

Table S12. Cartesian coordinates of the optimized geometry of $[B_{12}(CN)_{11}He]^-$ obtained at the B3LYP-GD3BJ/def2-QZVPP level.

Tag	Symbol	X	Y	Z

1	B	-1.511178	0.235344	0.593684
2	B	1.53032	-0.238174	-0.919272
3	B	-0.00041	-0.000194	1.519771
4	B	-0.690538	-1.36387	0.593912
5	B	-1.378121	-0.706599	-0.919044
6	B	-1.097404	1.092443	-0.919875
7	B	-0.243571	1.509443	0.594187
8	B	1.360534	0.697579	0.595066
9	B	0.699943	1.381727	-0.918725
10	B	0.000331	0.000151	-1.660725
11	B	0.246295	-1.528844	-0.919384
12	B	1.084015	-1.078221	0.593816
13	C	-0.461632	2.862417	1.263151
14	C	-2.027934	2.018524	-1.692574
15	C	-2.865318	0.446233	1.262498
16	C	-2.546189	-1.305691	-1.691891
17	C	-1.309494	-2.586341	1.263298
18	C	0.454819	-2.825186	-1.691762
19	C	2.055238	-2.044879	1.263009
20	C	2.827652	-0.440325	-1.69167
21	C	2.579876	1.322687	1.264361
22	C	1.293463	2.552972	-1.691048
23	C	-0.000773	-0.000384	3.045616
24	N	0.608566	-3.781493	-2.31028
25	N	-3.407857	-1.747516	-2.310793
26	N	-3.891735	0.606123	1.753903
27	N	-2.714181	2.701651	-2.31154
28	N	1.731468	3.416871	-2.309554
29	N	3.504229	1.79648	1.755961
30	N	-0.000968	-0.000354	4.194608
31	N	-1.778761	-3.512835	1.75521
32	N	-0.626768	3.887932	1.754706
33	N	2.791403	-2.777553	1.754769

34	N	3.784531	-0.589727	-2.310365
35	He	0.000589	-0.000572	-3.250672

Table S13. Cartesian coordinates of the optimized geometry of Na[B₁₂(CN)₁₁] obtained at the B3LYP-GD3BJ/def2-TZVPP level.

1	B	0.992557	-0.900332	0.373414
2	B	-1.895872	0.919847	0.141538
3	B	0.521912	0.000495	-1.095953
4	B	-0.375622	-1.463651	-0.635782
5	B	-0.478916	-1.492891	1.161311
6	B	0.394807	-0.001211	1.795869
7	B	0.992654	0.899706	0.374871
8	B	-0.375235	1.464494	-0.634094
9	B	-0.478625	1.491762	1.16315
10	B	-1.275157	-0.000695	1.443105
11	B	-1.896051	-0.919511	0.140551
12	B	-1.237074	0.000981	-1.257993
13	C	2.386609	1.535154	0.334118
14	C	1.084359	-0.002378	3.14932
15	C	2.386397	-1.535834	0.332647
16	C	-0.565842	-2.752115	2.006311
17	C	-0.27154	-2.752467	-1.437886
18	C	-3.200558	-1.697295	0.130754
19	C	-1.93476	0.001807	-2.609351
20	C	-3.20023	1.697873	0.132439
21	C	-0.270533	2.754038	-1.434919
22	C	-0.565057	2.750098	2.009487
23	C	1.587671	0.001143	-2.198376
24	N	-4.189014	-2.285178	0.139664
25	N	-0.618205	-3.701005	2.65418
26	N	3.493973	-1.786004	0.14661
27	N	1.631199	-0.003338	4.161205

28	N	-0.617038	3.69834	2.658336
29	N	-0.148333	3.72332	-2.042322
30	N	2.562091	0.001287	-2.809942
31	N	-0.149759	-3.721287	-2.046108
32	N	3.493957	1.7862	0.147803
33	N	-2.444824	0.00244	-3.64044
34	N	-4.188573	2.285939	0.141777
35	Na	4.468699	-0.000009	-1.264777

Table S14. Cartesian coordinates of the optimized geometry of Na[B₁₂(CN)₁₁Ne] obtained at the B3LYP-GD3BJ/def2-TZVPP level.

1	B	1.022599	-0.900654	0.478867
2	B	-1.725707	0.916321	-0.413752
3	B	0.910346	0.002365	-1.061001
4	B	-0.072948	-1.46107	-0.821549
5	B	-0.592764	-1.487235	0.899322
6	B	0.108623	-0.003345	1.717379
7	B	1.022416	0.899306	0.482529
8	B	-0.073154	1.464549	-0.815853
9	B	-0.592991	1.483913	0.905161
10	B	-1.453818	-0.002	1.012868
11	B	-1.725566	-0.914732	-0.417307
12	B	-0.765066	0.003321	-1.623652
13	C	2.3881	1.534384	0.767647
14	C	0.449468	-0.006425	3.198706
15	C	2.387905	-1.537189	0.762073
16	C	-0.884913	-2.740879	1.707522
17	C	0.215922	-2.749055	-1.579894
18	C	-3.000432	-1.686758	-0.71564
19	C	-1.130085	0.006143	-3.100878
20	C	-3.000783	1.689158	-0.709099
21	C	0.215599	2.755402	-1.569368

22	C	-0.88511	2.734366	1.718279
23	C	2.20347	0.003782	-1.885694
24	N	-3.975642	-2.264975	-0.909222
25	N	-1.10694	-3.677065	2.337784
26	N	3.507927	-1.789215	0.839539
27	N	0.720178	-0.00876	4.316621
28	N	-1.106909	3.668189	2.35212
29	N	0.47506	3.725595	-2.130251
30	N	3.293227	0.004372	-2.254585
31	N	0.475313	-3.717202	-2.144332
32	N	3.508199	1.785817	0.846078
33	N	-1.388891	0.00825	-4.221626
34	N	-3.976154	2.267832	-0.900493
35	Ne	-2.961472	-0.004687	2.312141
36	Na	4.779312	0.000521	-0.301802

S 6 Supplementary references

- 1 V. Geis, K. Guttsche, C. Knapp, H. Scherer and R. Uzun, *Dalton Trans.*, 2009, 2687–2694.
- 2 W. H. Knoth, H. C. Miller, J. C. Sauer, J. H. Balthis, Y. T. Chia and E. L. Muetterties, *Inorg. Chem.*, 1964, **3**, 159–167.
- 3 G. M. Sheldrick, *Acta Crystallogr., Sect. A: Found. Crystallogr.*, 2015, **71**, 3–8.
- 4 O. V. Dolomanov, L. J. Bourhis, R. J. Gildea, J. A. K. Howard and H. Puschmann, *J. Appl. Crystallogr.*, 2009, **42**, 339–341.
- 5 G. M. Sheldrick, *Acta Crystallogr. C Struct. Chem.*, 2015, **71**, 3–8.
- 6 E. Bernhardt, G. Henkel and H. Willner, *Z. Anorg. Allg. Chem.*, 2000, **626**, 560–568.
- 7 T. Küppers, E. Bernhardt, H. Willner, H. W. Rohm and M. Köckerling, *Inorg. Chem.*, 2005, **44**, 1015–1022.
- 8 Frisch, M. J. et al., *Gaussian 09, Revision D.01*, Gaussian, Inc., Wallingford CT, 2013.

- 9 M. Valiev, E. J. Bylaska, N. Govind, K. Kowalski, T. P. Straatsma, H.J.J. van Dam, D. Wang, J. Nieplocha, E. Apra, T. L. Windus and W. A. de Jong, *Comput. Phys. Commun.*, 2010, **181**, 1477–1489.
- 10 M. Mayer, V. van Lessen, M. Rohdenburg, G.-L. Hou, Z. Yang, R. M. Exner, E. Aprà, V. A. Azov, S. Grabowsky, S. S. Xantheas, K. R. Asmis, X.-B. Wang, C. Jenne and J. Warneke, *Proc. Natl. Acad. Sci. U.S.A.*, 2019, **116**, 8167–8172.
- 11 a) A. D. Becke, *J. Chem. Phys.*, 1993, **98**, 5648–5652; b) Lee, Yang and Parr, *Phys. Rev. B*, 1988, **37**, 785–789; c) B. Miehlich, A. Savin, H. Stoll and H. Preuss, *Chem. Phys. Lett.*, 1989, **157**, 200–206; d) A. D. McLean and G. S. Chandler, *J. Chem. Phys.*, 1980, **72**, 5639–5648; e) D. Rappoport and F. Furche, *J. Chem. Phys.*, 2010, **133**, 134105; f) F. Weigend and R. Ahlrichs, *Phys. Chem. Chem. Phys.*, 2005, **7**, 3297–3305;
- 12 S. Grimme, *J. Chem. Phys.*, 2003, **118**, 9095–9102.
- 13 a) T. H. Dunning, *J. Chem. Phys.*, 1989, **90**, 1007–1023; b) A. K. Wilson, T. van Mourik and T. H. Dunning, *J. Mol. Struct.*, 1996, **388**, 339–349;
- 14 N. Heine and K. R. Asmis, *Int. Rev. Phys. Chem.*, 2015, **34**, 1–34.
- 15 a) M. Brümmer, C. Kaposta, G. Santambrogio and K. R. Asmis, *J. Chem. Phys.*, 2003, **119**, 12700–12703; b) D. J. Goebbert, T. Wende, R. Bergmann, G. Meijer and K. R. Asmis, *J. Phys. Chem. A*, 2009, **113**, 5874–5880;
- 16 G. te Velde, F. M. Bickelhaupt, E. J. Baerends, C. Fonseca Guerra, S. J. A. van Gisbergen, J. G. Snijders and T. Ziegler, *J. Comput. Chem.*, 2001, **22**, 931–967.
- 17 F. M. Bickelhaupt and E. J. Baerends, in *Reviews in Computational Chemistry*, ed. K. B. Lipkowitz and D. B. Boyd, John Wiley & Sons, Inc, Hoboken, NJ, USA, 2000, vol. 15, pp. 1–86.